Beta Beams

Mats Lindroos

Mats Lindroos, ESS, Lund, Sweden and CERN, Switzerland

Mauro Mezzetto

INFN, Sezione di Padova

Key Words accelerators, charge conjugationparity (CP) violation, long-baseline neutrino experiments, neutrino oscillations, radioactive ions

Abstract The ultimate goal of neutrino oscillation physics will be the search for leptonic CP violation, requiring neutrino beams much more intense and pure of those used in the present generation of experiments. Beta beams are an attractive innovative possibility in this direction. Neutrinos are generated by the beta decays of radioactive nuclei and accelerated at very high energies. The resulting neutrino beam will consist of just one single flavor of neutrinos (ν_e or $\overline{\nu}_e$), easily predictable. A realistic beta beam design have already been demonstrated by the Eurisol Design Study, based on the CERN PS and SPS accelerators. The beta beam concept has been also extended in several other directions like high-energy, high-Q, electron-capture and low energy beta beams. Both the accelerator complex and of the physics potential of a neutrino experiment will be reviewed. Emphasis will be put on the beta beam design based on the CERN PS and SPS but other possibilities will be presented and discussed.

CONTENTS

Neutrino Oscillations . . . 3

Future Discoveries in Neutrino Oscillations . . . 3

Experimental Setups . . . 6

New Concepts on Neutrino Beams . . . 10

Machine aspects . . . 11

A possible beta-beam facility . . . 11

The beta-beam isotopes . . . 12

Ion transfer, Ionization and bunching . . . 14

Acceleration . . . 14

Beam losses . . . 15

Stacking and Storage . . . 15

Possible future development . . . 18

Acceleration of partly stripped ions . . . 19

CERN-FRÉJUS BETA BEAM PHYSICS POTENTIAL . . . 20

General principles . . . 20

The CERN-Fréjus Configuration . . . 21

Data Analysis . . . 22

Oscillation Analysis . . . 25

Combined Analyses with the Atmospheric Neutrinos . . . 26

Combined Analyses with the SPL Super Beam . . . 26

PHYSICS POTENTIAL OF OTHER BETA BEAM SETTINGS . . . 27

High Energy Beta Beams . . . 28

Beta Beams Based on ^{8}B *and* ^{8}Li *Ions* . . . 30

Monochromatic Neutrino Beams . . . 32

Low Energy Beta Beams . . . 33

Acknowledgments . . . 35

1 Neutrino Oscillations

The discovery of neutrino oscillations (1) has now established beyond doubt that neutrinos have mass and mix. This existence of neutrino masses is in fact the first solid experimental fact requiring physics beyond the Standard Model.

Neutrino oscillations are consistently described by three families ν_1, ν_2, ν_3 with mass values m_1, m_2 and m_3 that are connected to the flavor eigenstates ν_e, $\nu_\mu$and ν_τ by a mixing matrix U. The neutrino oscillation probability depends on three mixing angles, $\theta_{12}, \theta_{23}, \theta_{13}$, two mass differences, $\Delta m^2_{12} = m^2_2 - m^2_1$, $\Delta m^2_{23} = m^2_3 - m^2_2$, and a CP phase $\delta_{\rm CP}$. Additional phases are present in case neutrinos are Majorana particles, but they do not influence neutrino flavor oscillations at all.

1.1 Future Discoveries in Neutrino Oscillations

Three parameters (out of seven) have not yet been measured in neutrino oscillations.

The mixing angle θ_{13} is the key parameter of three-neutrino oscillations and regulates at the first order all the oscillation processes that could contribute to the measurement of sign(Δm^2_{23}) and $\delta_{\rm CP}$.

The neutrino mass hierarchy, the order by which mass eigenstates are coupled to flavor eigenstates, can be fixed by measuring the sign of Δm^2_{23}. Its value could be $+1$ (normal hierarchy), in which case ν_e would be the lightest neutrino, or -1 (inverted hierarchy), for which ν_e would be the heaviest. Its value is of great importance for double-beta decay experiments (2) and it could shed light on possible flavour symmetries.

The CP phase $\delta_{\rm CP}$ is the holy grail of ultimate neutrino oscillation searches.

The demonstration of CP violation in the lepton sector (LCPV) and the knowledge of the value of this phase would be crucial to understand the origin of the baryon asymmetry in the universe, providing a strong indication, though not proof, that leptogenesis is the explanation for the observed baryon asymmetry of the Universe (3).

All these parameters can be measured via subleading $\nu_\mu \to \nu_e$ oscillations that represent the key process of any future new discovery in neutrino oscillation physics.

1.1.1 Leptonic CP violation The phenomenon of CP (or T) violation in neutrino oscillations manifests itself by a difference in the oscillation probabilities of say, $P(\nu_\mu \to \nu_e)$ vs $P(\overline{\nu}_\mu \to \overline{\nu}_e)$ (CP violation), or $P(\nu_\mu \to \nu_e)$ vs $P(\nu_e \to \nu_\mu)$ (T violation).

Extensive studies, such as those published in a CERN yellow report (4), the European Network BENE (5) or the International Scoping Study (6) have been already performed to establish the physics potential of future facilities in discovering leptonic CP violation (7). When matter effects are not negligible, following Eq. (1) of (8), the transition probability $\nu_e \to \nu_\mu$ ($\bar{\nu}_e \to \bar{\nu}_\mu$) at second order in perturbation theory in θ_{13}, $\Delta m^2_{12}/\Delta m^2_{23}$, $|\Delta m^2_{12}/a|$ and $\Delta m^2_{12} L/E_\nu$ is:

$$P^{\pm}(\nu_e \to \nu_\mu) = X_\pm \sin^2(2\theta_{13}) + Y_\pm \cos(\theta_{13}) \sin(2\theta_{13}) \cos\left(\pm\delta - \frac{\Delta m^2_{23} L}{4E_\nu}\right) + Z\,, \tag{1}$$

where $\pm$ refers to neutrinos and antineutrinos, respectively. The coefficients of

the two equations are:

$$\begin{cases} X_{\pm} &= \sin^2(\theta_{23}) \left(\frac{\Delta m^2_{23}}{|a-\Delta m^2_{23}|}\right)^2 \sin^2\left(\frac{|a-\Delta m^2_{23}|L}{4E_\nu}\right) \ , \\ Y_{\pm} &= \sin(2\theta_{12})\sin(2\theta_{23}) \left(\frac{\Delta m^2_{12}}{a}\right)\left(\frac{\Delta m^2_{23}}{|a-\Delta m^2_{23}|}\right) \sin\left(\frac{aL}{4E_\nu}\right) \sin\left(\frac{|a-\Delta m^2_{23}|L}{4E_\nu}\right) \ , \\ Z &= \cos^2(\theta_{23})\sin^2(2\theta_{12}) \left(\frac{\Delta m^2_{12}}{a}\right)^2 \sin^2\left(\frac{aL}{4E_\nu}\right) \end{cases} \tag{2}$$

$a[\mathrm{eV}^2] = \pm 2\sqrt{2} G_F n_e E_\nu = 7.6{\cdot}10^{-5} \rho[g/cm^3] E_\nu[\mathrm{GeV}]$ changes sign by changing neutrinos with antineutrinos.

θ_{13} searches look for experimental evidence of ν_e appearance in excess of what is expected from the solar terms. The present limit on θ_{13}, mainly driven by the CHOOZ experiment at reactors (9), is $\sin^2\theta_{13} \leq 0.035$ (0.056), 90%CL (3σ) (10).

One of the interesting aspects of Eq. (1) is the occurrence of matter effects which, unlike the straightforward θ_{13} term, depend on the sign of the mass difference sign(Δm^2_{23}). These terms could allow extraction of the mass hierarchy, but could also be seen as a background to the CP violating effect, from which they can be distinguished by the different neutrino energy dependence.

The CP violation can be seen as interference between the solar and atmospheric oscillation for the same transition. Of experimental interest is the CP-violating asymmetry A_{CP}:

$$A_{CP} = \frac{P(\nu_\mu \to \nu_e) - P(\overline{\nu}_\mu \to \overline{\nu}_e)}{P(\nu_\mu \to \nu_e) + P(\overline{\nu}_\mu \to \overline{\nu}_e)} \tag{3}$$

displayed in Figure 1 as a function of θ_{13}, or the equivalent time reversal asymmetry A_T.

1.1.2 The problem of degenerate solutions

The richness of the $\nu_\mu \to \nu_e$ transition is also its weakness: it will be difficult to extract all the genuine parameters unambiguously. Due to the three-flavor structure of the oscillation probabilities, for a given experimental result several different disconnected regions

of the multi-dimensional space of parameters could fit the experimental data, originating degenerate solutions.

Traditionally these degeneracies are referred as the intrinsic or $(\delta_{\rm CP}, \theta_{13})$ degeneracy (8); the hierarchy or sign(Δm^2_{23})-degeneracy (12); the octant or θ_{23}-degeneracy (13). These lead to an eight-fold ambiguity in θ_{13} and $\delta_{\rm CP}$ (14), and hence degeneracies provide a serious limitation for the determination of θ_{13}, $\delta_{\rm CP}$, and sign(Δm^2_{23}).

1.2 Experimental Setups

1.2.1 Conventional neutrino beams Conventional neutrino beams are produced through the decay of π and K mesons generated by a high energy proton beam hitting small Z, needle-shaped, segmented targets. Positive (negative) mesons are sign-selected and focused (defocused) by large acceptance magnetic lenses into a long evacuated decay tunnel where ν_μ's ($\overline{\nu}_\mu$'s) are generated.

In case of positive charge selection, the ν_μ beam has typically a few percent of $\overline{\nu}_\mu$ contamination (from the decay of the residual π^-, K^- and K^0) and $\sim 1\%$ of ν_e and $\overline{\nu}_e$ coming from three-body $K^\pm$, K_0 decays and μ decays.

The precision of the evaluation of the intrinsic ν_e to ν_μ contamination is limited by the knowledge of the π and K production in the primary proton beam target requiring a devoted hadroproduction experiment. Recently the Harp experiment (15) measured both the K2K (16) and the MiniBooNE (17) targets, covering most of the useful pion phase-space, successfully improving the description of the two beam lines.

Close detectors are used to directly measure beam neutrinos and backgrounds (for a discussion about close detectors and systematic errors in future LBL ex-

periments see (18)).

Current long-baseline experiments with conventional neutrino beams can look for $\nu_\mu \to \nu_e$ transitions even if they are not optimized for such studies.

The K2K experiment published an analysis about ν_e appearance (19), still not improving the Chooz limit.

MINOS at NuMI (20) has already published preliminary results (21) showing a statistically not significant excess of ν_e-like events in the data sample.

The OPERA detector (22) at the CNGS (23) is also suited for electron detection, it can reach a 90% CL sensitivity of $\sin^2 2\theta_{13} = 0.06$ ($\Delta m^2_{23} = 2.5{\cdot}10^{-3}$ eV^2), (24), for five years exposure to the CNGS beam at nominal intensity of $4.5{\cdot}10^{19}$ pot/yr.

1.2.2 Second generation long-baseline experiments The focus of second generation LBL experiments will be the measurement of θ_{13} through the detection of sub-leading $\nu_\mu \to \nu_e$ oscillations.

The T2K (Tokai to Kamioka) experiment (25) will aim neutrinos from the Tokai site of J-PARC (30 GeV, 0.75 MW) to the Super-Kamiokande detector 295 km away. The neutrino beam is situated at an off-axis angle of 2.5 degrees, ensuring a pion decay peak energy of about 0.6 GeV. The beam line is equipped with a set of dedicated on-axis (INGRID) and off-axis (ND280) near detectors at a distance of 280 m. It is expected that the sensitivity of the experiment in a five-year ν_μ run at the full J-PARC beam intensity, will be of the order of $\sin^2 2\theta_{13} \leq 0.006$ (90% CL).

The NOνA experiment with an upgraded NuMI off-axis neutrino beam (26) ($E_\nu \sim 2$ GeV and a ν_e contamination lower than 0.5%), a totally active 15 kton liquid scintillator detector and with a baseline of 810 km (12 km off-axis), has

been approved at FNAL with the aim to explore $\nu_\mu \rightarrow \nu_e$ oscillations with a sensitivity 10 times better than MINOS.

1.2.3 Reactor experiments Another approach to searching for non-vanishing θ_{13} is to look at $\overline{\nu}_e$ disappearance using nuclear reactors as neutrino sources.

The Double Chooz (27) experiment will employ a far detector in the same location as the former CHOOZ detector as well as a near detector. The sensitivity after five years of data taking will be $\sin^2 2\theta_{13} = 0.025$ at 90% CL (27).

The Daya Bay project in China (28) could reach a $\sin^2 2\theta_{13}$ sensitivity below 0.01 integrating 70 times the statistics of Double Chooz .

A sketch of θ_{13} sensitivities as a function of the time, following the schedule reported in the experimental proposals, is reported in Figure 2.

1.2.4 Neutrino Super Beams Consensus exists that even a global fit of T2K plus NOνA plus reactors will not be able to provide firm results (3σ or better) about leptonic CP violation (30) or sign(Δm^2_{23}) (30, 31) whatever the value of θ_{13} . A further generation of long-baseline neutrino experiments will be needed to address this very important search in physics. As a rule of thumb they should be at least one order of magnitude more sensitive than T2K or NOνA a condition equivalent to an increase of two orders of magnitude on neutrino statistics, with a consequent important reduction of systematic errors.

To fulfill such a challenging improvement, conventional neutrino beams must be pushed to their ultimate limits (neutrino super beams) (32) and gigantic (megaton scale) neutrino detectors must be built.

Phase II of the T2K experiment, often called T2HK (33), foresees an increase of beam power up to the maximum feasible with the accelerator and target (4 MW beam power), antineutrino runs, and a very large, 520 kt, water Čerenkov

detector, HyperKamiokande or HK, to be built close to SuperKamiokande. An evolution of T2HK is the T2KK (34) project, where half of the HK detector would be installed in Japan, while the second half would be mounted in Korea, at a baseline of about 900 km, around the second oscillation maximum.

A wide-band beam (WBB) has been proposed at Fermilab upgrading the FNAL main injector after the end of the Tevatron programme (35). A conventional wide-band neutrino would be sent to a megaton water Čerenkov (or liquid argon) detector at the Homestake mine at a baseline of 1290 km. Wide-band beams possess the advantages of a higher on-axis flux and a broad energy spectrum. The latter allows the first and second oscillation nodes in the disappearance channel to be observed, providing a strong tool to solve the degeneracy problem (36). On the other hand, experiments served by wide-band beams must determine the incident neutrino energy with good resolution and eliminate the background from the high energy tail of the spectrum. The very long-baseline decreases the event rate at the far detector in an experiment where the statistics is very important and reduces the sensitivity of the experiment to θ_{13} and CP-violation.

1.2.5 CERN-SPL The CERN-SPL super beam is described in a little more detail for its possible synergy with the CERN-Fréjus beta beam, as discussed in Section 3.6. In the CERN-SPL super beam project (37) the planned 4MW SPL (Superconducting Proton Linac) would deliver a 3.5 GeV/c H^- beam on a Hg target to generate a neutrino beam with an average energy of ~ 0.3 GeV [1].

The ν_e contamination from K will be suppressed by threshold effects and the

[1] At present SPL is foreseen as one of the elements of a new injection chain for the SPS , in view of the LHC luminosity upgrades (38). In this context a power of 0.4 MW would be enough. Extensions to 4 MW could be driven by the needs of a neutrino super beam or a proton driver for a neutrino factory and/or a proton driver for EURISOL .

resulting ν_e/ν_μ ratio ($\sim 0.4\%$) will be known within 2% error. The use of a near and far detector (the latter at $L = 130$ km in the Fréjus area) will allow for both ν_μ-disappearance and $\nu_\mu \to \nu_e$ appearance studies. The physics potential of the SPL super beam (SPL-SB) with a water Čerenkov far detector with a fiducial mass of 440 kt, has been extensively studied (39, 40). The most updated sensitivity estimations for this setup have been published in Ref. (42) and are shown in Section 3.6.

The MEMPHYS (Megaton Mass Physics) detector (43) is a megaton-class water Čerenkov designed to be located at Fréjus, 130 km from CERN, addressing both the non-accelerator domain (nucleon decay, SuperNovae neutrino from burst event or from relic explosion, solar and atmospheric neutrinos) and the accelerator (super beam, beta beam) domain (44).

1.3 New Concepts on Neutrino Beams

The intrinsic limitations of conventional neutrino beams can be overcome if the neutrino parents are fully selected, collimated and accelerated to a given energy.

This can be attempted within the muon lifetime, bringing to the neutrino factory (45), or within beta decaying ion lifetimes, bringing to the beta beam(46, 47).

With this challenging approach several important improvements can be made to conventional neutrino beams:

- The neutrino fluxes would be simply derived from the knowledge of the number of parents circulating in the decay ring and from their Lorentz boost factor γ.
- The energy shape of the neutrino beam would be defined by just two param-

eters, the end-point energy Q_β of the beta decaying parent and its Lorentz boost factor γ.

- The intrinsic neutrino backgrounds would be suppressed (in the case of beta beam) or reduced to wrong sign muons (golden channel in neutrino factories).

The technological problems derive from the fact that the parents need to be unstable particles, requiring a fast, efficient acceleration scheme.

2 Machine aspects

2.1 A possible beta-beam facility

In the first beta-beam proposal (46, 48) the ions are produced in a thick target using a proton beam of 1-2 GeV, they are extracted as neutral atoms and re-ionized and bunched in a high frequency ECR source. The first step of acceleration is a linear accelerator which brings the ions to a kinetic energy of 150 Mega-electron-Volts (MeV) per nucleon. Subsequently, this beam is injected into a Rapid Cycling Synchrotron (RCS) in which the energy is increased to 500 MeV per nucleon. After this first step the beam enters the existing CERN accelerator complex and is first accelerated in the Proton Synchrotron (PS) to its maximum energy, transferred to the Super Proton Synchrotron (SPS) and finally ejected to a decay ring. The last step is done using a scheme which permits the "new" ions to be merged with the ions already circulating in the decay ring so that ions which still can decay (and create neutrinos) not are wasted and ejected from the decay ring too early. The details of each step in this scheme will be discussed below and an overview of the facility is shown in Figure 3. The key ingredient of

this setup is the re-use of existing accelerators to reduce cost and gain time for the construction of a beta-beam facility.

2.2 The beta-beam isotopes

2.2.1 Which isotope to use The CERN 2002 beta-beam study established a list of suitable isotopes considering life-time and contamination risk; this list is reprinted in Table 1 (β^- emitters) and Table 2 (β^+ emitters). For this first study ^{6}He and ^{18}Ne were selected; they have half lives at rest in the order of a second which corresponds to the typical cycling time of low energy accelerators (too long life-times will lead to large accumulated number of charges), they are easy to produce and are in gas phase at room temperature and they have no "dangerous" daughter products.

2.2.2 Isotope production Radioactive ions must be produced continuously as there is no way to stop them from decaying. There are two different methods used in modern Nuclear Physics for on-line production of exotic radioactive ions: the In-Flight (IF) method and the Isotope Separation On-Line (ISOL) method (50). The ISOL method uses a thick target in which a beam of particles is stopped. The thick target represents a high integrated cross section and the ISOL method will typically produce much higher intensity beams than the In-Flight method. To enhance diffusion and effusion out of the target it must be hot. For high intensity facilities the heating caused by the beam is more than sufficient and the challenge for the target designer is to get rid of the excess heat so that the target is not destroyed. There are a few variations of the ISOL method of interest for beta-beam and studies for the production of beta-beam relevant isotopes (see Table 3) have so far been done for: i) the converter method (51,52),

ii) direct production with a low energy projectile (53) and the recently proposed iii) production ring concept (54, 55).

The *converter method* makes us of a primary cooled target for the production of neutrons which in turn produces the isotope of interest in a secondary target. The neutrons are less destructive and delivers less heat for an equivalent production rate compared direct irradiation (with protons). The production of ^{6}He has been studied (51, 52) using the reaction `n + ⁹Be = ⁶He + ⁴He` which has a large cross section of some 100 mbarn. The *direct production method* makes use of the simplest way of creating a new isotope; accelerate one nucleus and merge it with another nucleus in a target at an energy high enough to overcome the Coulomb barrier but low enough to not destroy the newly formed nuclei through spallation or fission. The process has been studied for beta-beams (53) and to produce a sufficient number of ^{18}Ne isotopes for a beta-beam facility using a MgO solid target, 120 mAmps of primary ^{3}He beam at some 13 MeV of total energy is required. The *production ring concept* makes use of direct production with a very thin target placed in the closed orbit of a ion storage ring with continuous injection. The combination of energy loss in the transverse directions in the target with re-acceleration will result in a net beam cooling (54, 55) . In (54) a wedge shaped gas target is used in a dispersive region of the ring which adds longitudinal cooling. Furthermore, the proposed use of a gas target makes it possible to handle a large amount of beam power. The produced ions are collected with a second target downstream. In (55) a Fixed Field Alternating Gradient (FFAG) accelerator with large longitudinal acceptance is used to manage the beam without any longitudinal cooling. In both proposals the beam is injected partially stripped and the energy of the circulating ions are kept high enough to

assure that all of them emerge full stripped after the target. The production of ^{8}B and ^{8}Li with ^{3}He and Deuterium as projectiles and a liquid Lithium target (56) of enriched ^{6}Li or ^{7}Li has been proposed in (57) in which also a full six dimensional analysis of the cooling process is presented.

2.3 Ion transfer, Ionization and bunching

The ions produced in thick ISOL target have to be collected, ionized and bunched before they can be accelerated. The bunching is necessary for the injection into synchrotrons. An ECR source can operate either in afterglow or pre-glow mode (58) for ionization and bunching of ions. Tests of Pre-glow operation -in which neutral atoms are ionized and extracted in a pulse - for beta-beams have been performed within the EURISOL Design study (59) and further work is in progress within the EURONU Design study (60).

2.4 Acceleration

Accelerating a heavy ion is more challenging than accelerating a proton as the charge per mass unit (Q/A) is smaller and as the so called charge-exchange reactions are more severe. The first will make acceleration and transverse and longitudinal focusing more demanding while the latter will increase the losses during acceleration and storage.

The beam is first accelerated with a linac and the resulting semicontinuous beam is then injected into to the first synchrotron over a large number of turns. The combination of the chosen working point (Q) and a deliberate shift of the central beam orbit with dipolar magnets makes it possible to inject over as many as 50-100 turns with only moderate losses ($< 30\%$) (61).

2.5 Beam losses

The manipulation of the ion beam between the different accelerators for e.g. stripping and injection will induce losses. Furthermore, the collision with rest gas in the accelerator itself and the decay of radioactive ions will add to these losses. The lost ions can both induce radioactivity and cause vacuum degradation(62,63). For the beta-beam studied in (48) the arc lattice have been derived for ^{18}Ne and ^{6}He and large aperture dipoles (160 mm diameter) are used with such a length that all lost ions can be intercepted with absorbers after the dipole (64, 65). The choice of absorbers length and material is important as the absorbers could simply serve as a point for the ion to break up in a hadron cascade which could heat the following (superconducting) dipole badly (66). A possible way forward is to develop open mid-plane superconducting magnets (67). Another solution is to use a thick liner inside the dipole which would distribute the decay products over a larger volume of the magnet mass and coil. In the straight sections the decay products can successfully be kept in the machine and extracted to a beam dump before the arc (64).

2.6 Stacking and Storage

A bunched neutrino beam will enable an efficient suppression of background in the detector (see Section 3.3.2) and as the neutrino beam will be bunched if the ion beam is bunched (see Figure 5) it is necessary to use some form of stacking scheme for the incoming ion bunches; beam cooling is not an option as the cooling rate is too long.

The bunching can be expressed as a duty factor

$$\text{Duty factor} = \frac{N t_b}{T_{rev}} \tag{4}$$

were N is the number of filled bunches in the decay ring, t_b is the length of the individual bunch in seconds and the T_{rev} the revolution time. For a beta-beam facility operating at Lorenz $\gamma = 100$ using isotopes with an average neutrino energy spectrum of a few MeV at rest a duty factor not larger than 10^{-2} is required.

A longitudinal stacking scheme has been proposed in (68) in which the RF systems are used to stack from the center of each bunch. The outer parts of the bunch are for each injection cycle pushed outside the potential wall formed by the RF system and lost. This process has been simulated and tested in the CERN PS with very good results, see Figure 6. For the CERN beta-beam proposal (48) the merging can be done up to 15 times for an A/Q of 3 and up to 20 times for an A/Q of 2 where the longitudinal focusing is better. The efficiency of the merging will be further limited by the phase stability of the RF system. Assuming a realistic RF parameters and stability an overall stacking efficiency of 80% can be reached for both ^{6}He and ^{18}Ne (70). The total beam power injected is about 1 MJ for the reference facility and up to 50% of that beam power is lost from the bucket during stacking and has to be "scraped" away with longitudinal collimators. The decay ring (64) will have to be specially designed for this stacking scheme with a large dispersion region for the injection and another large dispersion region for beam collimation.

A further consideration for the decay ring design is the average (optical) beam divergence D in the straight sections. It can be estimated from the vertical and horizontal beam emittance ϵ and the Lorentz β:

$$D_{average} = \frac{\epsilon_{h,v}}{\beta_{average}}$$

2.6.1 Annual rate of neutrinos The purpose of the beta-beam facility is to produce a well collimated beam of single flavor electron (anti-)neutrino beams. For the ideal beta-beam facility in which all ions accelerated can be stored in the decay ring until they produce a neutrino and are lost the annual rate is simply equal to the number of ions injected.

For the case in which the decay ring only can stack a certain number of bunches the upper intensity limit in the machine can be calculated from the truncated series of repeated injections in the decay ring. In Figure 7 the actual fraction of stored ions compared to the ideal case in which all injected ions are stored in the ring is plotted as function of the number of "merges" for both ^{6}He and ^{18}Ne. Note that for the realistic case of only 15 merges for ^{6}He and 20 merges for ^{18}Ne only corresponds to an efficiency of the stacking scheme of 54% and 26% respectively. The annual rate at the end of one of the straight sections for a snow mass year (71) of 10^7 seconds with the relative length of the straight section (f) compared to the circumference of the ring can be written as:

$$A = 10^7 f \frac{N}{T} \left(1 - e^{-\lambda n T}\right) \tag{5}$$

where N is the number of ions per injection into the decay ring, T the time interval between injections, λ the decay constant and n the number of number of 100% efficient merges. Note that this is the **maximum** annual rate as it assumes perfect stacking from the center of the bunch. The decay constant (λ) for the radioactive decay producing neutrinos in the right energy interval is not necessarily the only decay constant determining the decay-rate of the ions in the decay ring. There might be other loss processes such as vacuum collisions - resulting in a change of mass-to-charge ratio of the ion. For monochromatic neutrino beams from electron capture decay there is often a radioactive branch

of competing $\beta+$ decay with a different decay constant. The annual rate of the beta-beam facility studied in (48) is assumed to reach 1.1×10^{18} electron neutrinos per year from the decay of ^{18}Ne and and 2.9×10^{18} electron anti-neutrinos per year from the decay of ^{6}He. To reach this ambitious goals a production rate of 2×10^{13} ions per second of each species are required. The overall efficiency from the ion source to the number of ions injected into the decay ring is assumed to reach 12% for ^{18}Ne and 25% for ^{6}He. Using the previously quoted efficiencies for the stacking scheme the total efficiency from the ion source to ions decaying in one straight section (which is 36% of the total circumference) is 1% and 5% respectively.

2.7 Possible future development

It is apparent from physics reach studies that if the annual rate, energy or energy resolution of the neutrinos could be increased the beta-beam concept would have a larger scope.

New particles can only be injected once the magnets in a synchrotron are back to the field corresponding to the injection energy. The simplest way to make use of this lost production time is to *accumulate the ions produced in this interval.* A study has been done for the CERN 2002 beta-beam (72) using a low-energy storage ring with a gain of up to a factor of five in the overall annual rate.

In principle, the *two types of ions* can be kept at the same time in the decay ring. The ions would be kept in different bunches sufficiently well separated in time. This scheme will impose a fixed relationship between the γ of the two isotopes, it will require very large aperture dipoles, it will need "double injectors" for both ion types and an a highly complex RF system for the accumulation

process.

A conceptual study was done at FermiLab for a higher gamma of 300 using the Tevatron as the pre-accelerator (49). The opening angle of the kinematic focusing angle will change with gamma ($\Theta \approx 1/\gamma$), the isotope life time will be longer due to increased time dilatation and the decay ring will have to be larger or the dipole magnets more powerful (see Table 4) to cope with the increased magnetic rigidity of the radioactive ions.

2.8 Acceleration of partly stripped ions

Proton rich isotopes decaying through electron capture can be used to create a mono energetic neutrino beam (73, 74). The equivalent process on the neutron rich side is bound beta-decay. The branching rate for this process in generally very small but it could be used for a mono energetic anti-neutrino beam (75).

A definite requirement for electron capture decay is that the nuclei only is partly stripped so that there is an electron available for capture. At high energy the likelihood to pick-up an electron is vanishingly small. However, the likelihood of losing an electron will, expressed in an equivalent half life, be in the order of minutes in a ring with a modern ultra high vacuum system. The modified annual rate for a snow mass year can be written as,

$$Rate = \frac{Nf}{T} \times \frac{\lambda_{ec}/\gamma_{top}}{\lambda_{ec}/\gamma_{top} + \lambda_{vac}} \times \left(1 - e^{-mT(\lambda_{ec}/\gamma_{top}+\lambda_{vac})}\right) \times 10^7$$

where N is the number of incoming ions into the decay ring per injection cycle, f the fraction of the decay ring being a straight section pointing towards the detector and T the time between injection cycles.

The combination of the high charge state, the longer half-life and the electron stripping losses would even with exceptionally short-lived and electron capture

decaying rare-earth isotopes (76) require a large number of ions to be accelerated and stored in the decay ring to keep the annual rate high. For cases studied in (77) the tune shift in the CERN accelerators PS and SPS would peak well above 0.25 to keep the annual rate at 10^{18} electron neutrinos at the end of one straight section for a snowmass year.

3 CERN-FRÉJUS BETA BEAM PHYSICS POTENTIAL

3.1 General principles

A beta beam is produced from the decay of a high energy radioactive ion beam, resulting in a pure ν_e or $\bar{\nu}_e$ beam. The flavor transitions that can, in principle, be studied in this facility are:

$$\nu_e \to \nu_\mu \qquad \nu_e \to \nu_e \qquad \nu_e \to \nu_\tau$$

$$\bar{\nu}_e \to \bar{\nu}_\mu \qquad \bar{\nu}_e \to \bar{\nu}_e \qquad \bar{\nu}_e \to \bar{\nu}_\tau.$$

In the laboratory frame, the neutrino flux, $\Phi^{\rm lab}$, is given by:

$$\left.\frac{d\Phi^{\rm lab}}{dSdy}\right|_{\theta\simeq 0} \simeq \frac{N_\beta}{\pi L^2}\frac{\gamma^2}{g(y_e)}y^2(1-y)\sqrt{(1-y)^2-y_e^2} \tag{6}$$

where N_β is the number of ion decays per unit time, Q_β is the endpoint kinetic energy of the beta particle, γ is the relativistic Lorentz boost factor, m_e is the mass of the electron, dS is the element of solid angle, L is the distance between the decay ring and the detector, $0 \leq y = \frac{E_\nu}{2\gamma Q_\beta} \leq 1 - y_e$, and $y_e = m_e/Q_\beta$; and

$$g(y_e) \equiv \frac{1}{60}\left\{\sqrt{1-y_e^2}(2-9y_e^2-8y_e^4)+15y_e^4\log\left[\frac{y_e}{1-\sqrt{1-y_e^2}}\right]\right\} \tag{7}$$

The intensity and the energy shape of the neutrino beam are determined by just four quantities: N_β, Q_β, γ, L. Once these parameters are fixed, the neutrino flux

can be calculated precisely since the kinematics of β decay is very well-known (79).

There are some approximate scaling laws at the varying of the parameters (assuming N_β constant): the maximum γ to which a given accelerator can accelerate a ion is proportional to Z/A. For instance, if SPS can accelerate protons up to 450 GeV, ^{6}He $(Z/A = 2/6)$ can be accelerated up to $\gamma = 150$.

The neutrino flux Φ at a far detector placed at a distance L is:

$$\Phi \propto \frac{\gamma^2}{L^2}$$

because the emission angle of the neutrino from the parent ion, in the laboratory frame, is proportional to γ^{-1}.

Since the optimal distance L is defined by the oscillation Δm^2: $L \propto E_\nu/\Delta m^2$ and $E_\nu \propto \gamma Q_\beta$ the flux becomes

$$\Phi \propto \frac{(\Delta m^2)^2}{Q_\beta^2}.$$

Considering that the neutrino interaction rate I at the far detector is $I = \sigma\Phi$ and that the neutrino cross section σ goes as $\sigma \propto E_\nu$ (this scaling law becomes inaccurate for $E_\nu < 5$ GeV) a merit factor $\mathcal{M}$ can be derived

$$\mathcal{M} \propto \frac{\gamma}{Q_\beta}. \tag{8}$$

It follows that performances of a beta beam scale as the Lorentz boost factor γ and are inversely proportional to the endpoint energy Q_β of the parent ions.

3.2 The CERN-Fréjus Configuration

The CERN beta beam can accelerate ^{6}He ions up to $\gamma = 150$ and ^{18}Ne ions up to $\gamma = 250$. Given the characteristics of the ^{6}He decay, this translates to mean

neutrino energies of up to ~ 600 MeV, equivalent to a maximum baseline of 300 km.

The only realistic candidate site for the excavation of a megaton class detector fitting this request is the Fréjus site, at a distance of 130 km.

To fit this distance the optimal γ for ^{6}He is $\gamma \simeq 100$. Higher γ values would increase interaction rates in the detector, but not the oscillated event interaction rates by very much, since the baseline would no longer fit the oscillation pattern. Furthermore background rates would rise, as discussed in Section 3.3.2.

Smaller γ values would have the advantage of suppressing background rates in the detector, $\gamma_{^6\mathrm{He}} = 66$ had been indeed the initial choice for the CERN-Fréjus configuration (80, 81) for this reason. Under this condition however the neutrino flux is smaller and a bigger fraction of ν_μ events created by oscillations produces a muon below the Čerenkov light production threshold ($p_\mu > 120$ MeV/c).

The CERN-Fréjus configuration (CFBB) is not designed to be the absolute optimal configuration for a beta beam experiment. It is intended to be a realistic setup where both the beam and the detector sites are chosen among realistic conditions.

3.3 Data Analysis

The most sensitive process in a beta beam experiment are $\nu_e \to \nu_\mu$ transitions as will be discussed in Section 3.4.

They introduce an experimental problem never faced so far, the detection of a small content of ν_μ events in a pure ν_e beam. This process can be complemented by $\nu_e \to \nu_e$ transitions, where a small deficit in ν_e spectrum is looked for.

The combination of the two processes demands a massive detector capable of

measuring with precision and high purity both electrons and muons, the natural baseline option is the MEMPHYS detector.

3.3.1 Signals The neutrino flux in this setup is shown in Fig. 8.

In this energy range almost all the neutrino charged-current interactions are quasi-elastic interactions (QE), a two-body configuration very favorable for a water Čerenkov detector because the neutrino energy can be derived by just measuring the momentum and the direction of the outgoing lepton. The precision in measuring the neutrino energy is shown in Fig 9. The energy of single ring non-quasi-elastic events results underestimated, because of the different kinematics. This effect is hardly visible in the low energy bins, where the non-quasi-elastic event fraction is small. The non-gaussian features of energy reconstruction are taken into account by using migration matrices connecting true and reconstructed neutrino energy, as discussed in (42).

Data reduction is shown in Fig. 10 for ^{18}Ne events.

3.3.2 Backgrounds While a beta beam provides an absolutely clean beam of $\nu_e(\overline{\nu}_e)$, backgrounds can be produced by imperfect performances of the neutrino detector.

The experimental sensitivity requires that the electron-muon mis-identification rate in the detector must be kept below 10^{-4}. This can be guaranteed by a water Čerenkov detector thanks to the particle identification algorithms based on the very different topologies of muons and electrons rings. Furthermore a muon can be positively identified by detecting its decay in a Michel electron (the probability for a negative muon to be captured before decay is 22% in water).

The charged pions produced in resonant neutrino-nucleus interactions can also be mis-identified as muons, generating backgrounds. At the CERN Fréjus ener-

gies anyway the pion production is suppressed just because just below or close to the threshold (337 MeV/c), and because the outgoing pion, to be detectable in water, must have a momentum greater than 159 MeV/c. Furthermore the largest part of negative pions is absorbed before the completion of the decay chain.

Atmospheric neutrinos are another source of background in a beta beam experiment. The spectrum of ν_μ and $\overline{\nu}_\mu$, shown in Fig. 8 right, overlaps the spectrum of oscillated signals, providing a copious source of backgrounds. The direction of the outgoing muon is not a strong enough constraint to eliminate this background because both the quasi-elastic kinematics and the Fermi motion generate a loose correlation between the outgoing lepton and the incoming neutrino. At the energies of the $\gamma = 100$ beta beam, the angular resolution is about 0.25 radians. So the only other handle against atmospheric neutrinos is to keep the time in which beam neutrinos arrive to the detector very short, in other terms the duty cycle of the beta beam decay ring must be very short. As computed in (82, 83) a duty cycle of 10^{-2} is needed to keep the atmospheric neutrino background rate below the NC pion background rate.

It is worth noting that the fraction of background events with respect to the fully oscillated sample, after the analysis selection, is about 0.2%, well below the $\sim 1\%$ characteristic of super beam experiments. Furthermore these backgrounds (Fig. 10) have a different spectral distribution from oscillated events, reducing their impact on oscillation analysis, as will be discussed in Section 3.4.1.

For an independent computation of backgrounds in a beta beam setup see (84)

3.4 Oscillation Analysis

Most of the results shown in the following are taken from (42), assuming a detector mass of 440 kt, a running time $(\nu + \bar{\nu})$ of 5 + 5 yr, a beam intensity of $2.9\,(1.1) \cdot 10^{18}$ ^{6}He (^{18}Ne) dcys/yr and a conservative 5% for the systematic errors.

3.4.1 $\boldsymbol{\theta_{13}}$ SEARCHES Non-zero values of θ_{13} are looked for by exploiting $\nu_e \to \nu_\mu$ transitions, the discovery limits (computed with the help of the Globes software (86)) are shown in Fig. 11 left. The main limiting factor for the beta beam performances is the statistics. The impact of systematics is very small, one finds that systematical errors dominate ($\sigma_{\rm bkgr}\sqrt{B} > 1$) if $\sigma_{\rm bkgr} \gtrsim 6\%$.

Also $\nu_e \to \nu_e$ transitions contribute to the θ_{13} sensitivity. They are however marginal if the overall systematic error is around 2% (as a comparison reactor experiments plan to reach systematic errors of about 0.2% in $\overline{\nu}_e$ disappearance just to reach sensitivities of $\sin^2 2\theta_{13} \simeq 0.01$). As computed in (40), the CFBB experiment could reach sensitivities of $\sin^2 2\theta_{13} \leq 0.02$ (90% CL) to ν_e disappearance.

3.4.2 LEPTONIC CP VIOLATION SEARCHES Leptonic CP violation searches are performed by comparing event rates and spectra in neutrino and antineutrino runs, as discussed in Section 1.1.1.

It is important to note that in the specific setup of CFBB, where matter effects are negligible and so no other process is in competition with LCPV to generate differences between neutrino and antineutrinos, the simple comparison of neutrino and antineutrino oscillation rates can provide evidence of LCPV independently from any neutrino oscillation model.

The LCPV discovery potential is shown in Fig. 11 center.

3.5 Combined Analyses with the Atmospheric Neutrinos

Beta beam and atmospheric neutrino data are a truly synergic combination, in that together the two samples provide more information than expected just from statistics (87). Beta beam has very limited capabilities in measuring sign(Δm^2_{23})and resolving degeneracies on the other hand atmospheric neutrinos, even if measured with large statistics, cannot measure sign(Δm^2_{23})in the absence of a measured value of θ_{13} , precisely what beta beam measures at best.

The combination of ATM+beta beam data (42) leads to a non-trivial sensitivity to the neutrino mass hierarchy, i.e. to sign(Δm^2_{23})as shown in Fig. 11 right. For beta beam data alone there is practically no sensitivity in the CFBB setup because of the very small matter effects due to the relatively short baseline. However, by including data from atmospheric neutrinos the mass hierarchy can be identified at 2σ CL provided $\sin^2 2\theta_{13} \gtrsim 0.03 - 0.04$.

Atmospheric data help also very much in breaking degeneracies as discussed in (42).

3.6 Combined Analyses with the SPL Super Beam

Soon after the first proposal of beta beams (46) it was realized that neutrinos created by the SPL could be fired to the same detector (40, 41).

The injector of a beta-beam complex must be a 1 - 3 GeV Linac, precisely the energy of the SPL. Furthermore radioactive ion production requires at most 0.2 MW, while SPL could deliver up to 4 MW of power.

Under these circumstances a very intense super beam, already discussed in Section 1.2.5, can run together with a beta beam. The typical energy of a neutrino beam created by the SPL can nicely match the energy of a $\gamma = 100$ beta beam

(see Fig. 8) so the two neutrino beams can share the same baseline, thus the same detector, combine performances are shown in Fig. 11.

The combination of a super beam with a beta beam in the same experiment can provide an experimental environment with very unique characteristics:

- The two beams can be used to separately study CP channels like $\nu_\mu \to \nu_e$ vs $\overline{\nu}_\mu \to \overline{\nu}_e$ and $\nu_e \to \nu_\mu$ vs $\overline{\nu}_e \to \overline{\nu}_\mu$.
- They can be mixed to study T transitions like $\nu_\mu \to \nu_e$ vs $\nu_e \to \nu_\mu$ and $\overline{\nu}_\mu \to \overline{\nu}_e$ vs $\overline{\nu}_e \to \overline{\nu}_\mu$.
- They can be mixed to study CPT transitions like $\nu_\mu \to \nu_e$ vs $\overline{\nu}_e \to \overline{\nu}_\mu$ and $\nu_e \to \nu_\mu$ vs $\overline{\nu}_\mu \to \overline{\nu}_e$.

The addition of a super beam to a beta beam could also complement some of the weak points of the beta beam, namely the lack of sensitivity to the atmospheric parameters θ_{23} and Δm^2_{23} and the lack of ν_μ events in the close detector, useful for calibrating beta beam signal efficiency and measuring the ν_e/ν_μcross section ratio.

In an SPL super beam+beta beam experiment all the channels would be measured in the same detector with small background rates. This is highly beneficial for systematic errors and would provide redundancy in the oscillation signals, a feature that should not be underestimated in an experimental field that today is completely unexplored.

4 PHYSICS POTENTIAL OF OTHER BETA BEAM SETTINGS

Several different new concepts have been developed to explore the full capabilities of a beta beam setup, aiming to higher neutrino fluxes to higher neutrino ener-

gies, to introduce innovative tools in neutrino oscillation searches and to measure neutrino properties in the 10-100 MeV energy range.

4.1 High Energy Beta Beams

High energy beta beams (HEBB) have been introduced by (85), where the final accelerator is designed to accelerate ^{6}He up to $\gamma = 350$ (2.3 times higher that the maximum $\gamma(^6\text{He})$ reachable at the SPS), a condition fulfilled by an accelerator capable of accelerating protons at 1 TeV. The same number of ion decays/year as the CFBB has been considered [2].

Two major upgrades of the accelerator scheme are needed for high energy beta beams. Of course a new accelerator is needed. Proton accelerators at 1 TeV energy have been recently dismantled (HERA at Desy) or are going to be shut-down (Tevatron at Fermilab). The LHC is a collider with a very slow acceleration cycle which makes it unsuitable for the acceleration of the large number of radioactive ions required for a beta beam. A possible energy upgrade of the LHC would require a new higher energy injector, SPS+ (38), which could be used for a higher energy beta-beam.

Also the decay ring is heavily affected by a γ increase of the stored ions as shown in Table 4.

Important advantages of a high energy beta beam are the greater statistics (cfr. the beta beam merit factor Eq. 8) and the possibility to increase the baseline length to the point where sensitivity to sign(Δm^2_{23}) becomes sizable.

Reference (88) studies the case of a $\gamma = 350$ beta beam fired to a water Čerenkov detector at about 700 km. As discussed in Section 3.3.1), by in-

[2] in a super beam setup this would be equivalent to a power increase of a 2.3 factor

creasing the average neutrino energy, the fraction of well reconstructed events decreases, until the point where the flux increase provided by the higher gamma is vanished by the loss of QE events. According to (88) this happens for $\gamma \simeq 400$.

Backgrounds from NC are much more in HEBB than in CFBB, but they cluster at small energies. As demonstrated by Ref. (88), a simple lower cut in the visible energy keeps NC backgrounds to a tolerable level. Also atmospheric neutrinos integrated in the signal energy range increase, but much less than signal events, when compared to CFBB. This feature implies that in HEBB the bounds to the beta beam duty cycle derived from the atmospheric neutrino background rate are less severe, allowing for higher duty cycles.

Following the results of (88) a $\gamma = 350$ beta beam would be definitely better than CFBB but only marginally better (as far as θ_{13} and LCPV sensitivities are concerned) than an SPS-based beta beam at the maximum γ ($\gamma = 150$ for ^{6}He and ^{18}Ne) and at the optimal baseline (L=300 km).

For a comparison of beta beam setups at different γ see also (89).

As emerges from the above discussion, a water Čerenkov detector shows some limitation in the energy range of high energy beta beam, if only quasi-elastic events can be efficiently reconstructed. To overcome this problem different detector technologies have been taken into account for HEBB.

In (90), the case of a totally active scintillating detector (TASD), derived from the NOνA project, has been considered. An interesting study of (90) is the scaling of performances with the number of ion decays/year (either this number or its product with the γ factor could be assumed constant) showing that the assumptions about the scaling law are very important for the overall comparisons.

A different detector technology has been considered in (91): an iron calorime-

ter, where the sensitive elements (2 cm thick glass RPC planes with a 2 mm gas filled gap) are interleaved with iron plates (4 cm thick). This configuration has the advantage of providing a higher density than a TASD detector, such that a 40 kt detector could fit a present LNGS hall, a very attractive experimental situation. A full simulation of this detector has been performed, allowing for a robust sensitivity estimation. The fraction of NC backgrounds with respect to the non-oscillated ν_e events is 8.8×10^{-3} at $\gamma = 580$, a much higher rate than the 10^{-3} rate assumed (but not computed) at $\gamma = 500$ for a TASD detector.

Overall performances of this setup almost match those of the CERN-Fréjus scenario, again assuming a constant ion decay rate. Combined sensitivity with atmospheric neutrinos of this setup have been also studied in (92).

4.2 Beta Beams Based on ^{8}B and ^{8}Li Ions

^{8}B and ^{8}Li ions have a significantly higher Q_β value than ^{6}He and ^{18}Ne as can be derived from Table 1, 2. In Section 3.1 it has already been shown that higher Q_β ions can allow greater neutrino energies for the same γ:

$$E_\nu^{\max} = 2\gamma Q_\beta \tag{9}$$

Furthermore the Z/A of the ^{8}B /^{8}Li ions are higher than the formers': such that considering the β^- emitters they could produce a neutrino beam 4.74 times more energetic than a ^{6}He /^{18}Ne beam, for the same accelerator energy, with a shorter decay ring length. On the other hand the merit factor of a ^{8}B /^{8}Li beam (see Section 3.1) is smaller than a ^{6}He /^{18}Ne beam since it is inversely proportional to Q_β and so it would produce smaller fluxes at the same neutrino energy. About four times more ions are needed to allow a ^{8}B /^{8}Li beta beam to match the performances of a ^{6}He /^{18}Ne beta beam at the same γ (83).

In (54), as discussed in Section 2.2.2, an innovative procedure has been proposed to produce ^{8}B /^{8}Li ions, in principle capable of producing 2 - 3 orders of magnitude more radioactive ion fluxes. Feasibility and performances of this injection scheme will be studied in the context of the European Design Study EUROnu (60).

The physics case of a ^{8}B /^{8}Li beta beam based on the Fermilab Main Injector and a massive liquid argon detector at Soudan has been discussed in (93) a setup based on the Tevatron and the detector at DUSEL has been studied in (94).

The authors of (95) have studied the case of a mixed ^{8}B /^{8}Li and ^{6}He /^{18}Ne beta beam, based on SPS. A 500 kt water Čerenkov detector with a baseline of about 700 km would receive the ^{8}B /^{8}Li beta beam at the first oscillation maximum and the ^{6}He /^{18}Ne beta beam at the second oscillation maximum. The same ion decays/year of CFBB are assumed also for ^{8}B and ^{8}Li. This setup has little or null advantage as far as θ_{13} and LCPV are concerned, while it outperforms CFBB as far as sign(Δm^2_{23}) sensitivity is concerned.

Along this line it is also interesting to note the study of reference (96) where the case of a single ^{18}Ne exposure is considered at $\gamma = 450$ (within the reach of the SPS+) and with a 50 kt iron detector placed at a baseline of 1050 km (CERN-Boulby mine).

The combination of high energy, ^{8}B /^{8}Li based, beta beams allows the so called "magic baseline" $L_{\rm magic}$ to be covered.

The concept of a magic baseline (14, 97) derives from the observation that in Eq.(1) for $\rho L = \sqrt{2}\pi/G_F Y_e$ (Y_e is the electron fraction inside the earth) any $\delta_{\rm CP}$ dependence disappears from $P_{e\mu}$ allowing sign(Δm^2_{23}) effects to be measured without any degenerate solution.

According to the Preliminary Reference Earth Model PREM (98) earth matter density profile, $L_{\rm magic} \simeq 7690$ km, the resonance energy for matter effects would be:

$$E_{\rm res} \equiv \frac{|\Delta m^2_{31}| \cos 2\theta_{13}}{2\sqrt{2} G_F N_e} \simeq 7 \text{ GeV} \tag{10}$$

for $|\Delta m^2_{31}| = 2.4 \cdot 10^{-3}$ eV^2 and $\sin^2 2\theta_{13} = 0.1$.

It is important to note that close to matter resonance, the flux of oscillated events at the detector roughly falls as a function of $1/L$ (against the $1/L^2$ fall of vacuum oscillations), which means that longer baselines might be preferred.

Studies of beta beams at the magic baselines have been initiated (99) within the context of the India-based Neutrino Observatory (INO) (100), where a large magnetized iron calorimeter (ICAL) is set to come up. The CERN-INO distance approaches the magic baseline, being 7152 km. It has to be noted anyway that the slope at which the decay ring should be built to point at a 7000 km far detector is about 34.5°, such that it seems very challenging to built it.

Two detectors at two different distances are anyway needed, since the detector at the magic baseline is blind to any LCPV effect by construction, this kind of setup has been studied in (101–103)

The potentialities of a high-γ-high-Q beta beam result to be extremely promising (102, 104).

4.3 Monochromatic Neutrino Beams

Monochromatic neutrino beams based on the electron capture process (ECB), see also Section 2.8, are certainly an intriguing experimental setup, but for LCPV searches they have two major apparent limitations: there is no way to have antineutrino beams (a conceptual possibility for the production of monochromatic

neutrino beams is discussed later in this section) and they miss spectral information, which is very important to solve degeneracies.

To overcome these limitations interesting experimental strategies have been introduced.

In (73,105) it has been proposed to study θ_{13} and LCPV in a ECB setup based on the ^{150}Dy ion (3.1 min lifetime and $Q = 1794$ keV) running the beam at two γs tuned to the first and the second oscillation maximum. Performances of ECB in these configurations are very promising.

Reference (106) proposes a more aggressive strategy, based on $^{110}_{50}Sn$ isotopes ($Q = 267$ Kev and 4.11 h lifetime), at $\gamma = 2500$ and a baseline of 600 km.

A way to generate monochromatic antineutrino beams has been delineated in (75) . It is based on the process of the bound-state β decay (107) where the electron is created in a previously unoccupied bound atomic state and the antineutrino is emitted at a fixed energy. Candidates exist like $^{108}_{47}Ag^{46+}$ with $\tau_{1/2} = 24.4$ s and neutrino energies of 1.90 and 1.67 MeV for the EC and bound-beta lines respectively, but it should be noted that the branching ratios for such processes are of about 1%, making it very difficult even conceptually to produce significant neutrino fluxes.

4.4 Low Energy Beta Beams

Beta beams are the ideal tool for measuring neutrino cross sections, since the neutrino beam flux can be predicted with high precision. This particular feature has been extensively discussed in the literature for neutrino energies around 100 MeV, where a wide set of interesting non-oscillation neutrino experiments is possible.

In (108) it was proposed to build a low energy facility in the 100 MeV energy range for nuclear structure studies and neutrino-nucleus interactions (108–112), electroweak tests of the Standard Model (108, 113–115) as well as core-collapse Supernova physics (108, 116, 117).

In this energy range the decay ring characteristics and the detector locations have to be re-optimized, as discussed in (108, 109, 118, 119).

Neutrino-nucleus interactions represent a topic of current great interest for various domains of physics, from neutrino physics to nuclear physics and astrophysics. The motivations come for example from the need for a precise knowledge of the neutrino detector response in neutrino experiments and in core collapse supernova observatories aiming at the detection of the relic supernova neutrino background (44) using neutrino interaction on argon (120) and carbon or oxygen (121) or of neutrinos from an (extra)galactic explosion (44).

For instance, the 1n or 2n emission associated with charged-current events in a supernova lead-based observatory depends on the average electron neutrino energy, which encodes information on the still unknown third neutrino mixing angle θ_{13} (122).

Neutrino-nucleon reactions play a crucial role in the understanding of the supernova dynamics (123,124), the yields of the r-process nucleosynthesis that could take place in such environments (125) and also contribute to the energy transfer (from accretion-disk neutrinos to nucleons) in gamma-ray burst models (126,127). Finally, understanding the subtleties of the neutrino-nucleon interactions is important to the terrestrial observation of neutrino signals (128, 129).

Besides the astrophysical applications, a precise knowledge of the nuclear response of neutrinos is also crucial for our knowledge of the nuclear isospin and

spin-isospin response that has fundamental implications, for example the search of physics beyond the Standard Model through neutrinoless double-beta decay (111).

Several applications for fundamental interaction studies of low energy beta beams have been discussed so far: the measurement of the Weinberg angle at low momentum transfer (114), a conserved vector current (CVC) test with neutrino beams (115), the measurement of the neutrino magnetic moment (110), the measurement of coherent neutrino-nucleus elastic scattering (130), the sensitivity to extra neutral gauge bosons, leptoquarks and r-parity breaking interactions (131), the search for sterile neutrinos (132).

For a more detailed discussion about physics at a low energy beta beam see the topical review published by Cristina Volpe (133).

5 Acknowledgments

Many thanks to all our colleagues in the world wide neutrino physics community. A special thanks to all our colleagues in the beta beam task group in the EC supported EURISOL Design Study and in the EC supported BENE (within the Infrastructure Activity CARE) and EUROnu networks. Special thanks to Thomas Schwetz for his kind help in preparing some of the physics potential plots.

The authors wish to thank their home institutes, Lund University and CERN for Mats Lindroos and Istituto Nazionale di Fisica Nucleare for Mauro Mezzetto, for supporting this work. Mats Lindroos also wishes to thank the Physics Department at the University of Liverpool where he is Visiting Professor for their support.

We acknowledge the financial support of the European Community under the FP6 Research Infrastructure Action Structuring the European Research Area EURISOL DS Project Contract No. 515768 RIDS.

We acknowledge the financial support of the European Community under the European Commission Framework Programme 7 Design Study: EUROnu, Project Number 212372. The EC is not liable for any use that may be made of the information contained herein.

:

Literature Cited

1. Fukuda Y et al. (Super-Kamiokande Collaboration), Phys. Rev. Lett. 81 (1998) 1562.
2. Feruglio F, Strumia A and Vissani F, Nucl. Phys. B 637 (2002) 345 [Addendum-ibid. B 659 (2003) 359].
3. Fukugita M and Yanagida T, Phys. Lett. B 174 (1986) 45.
4. Blondel A et al., CERN-2004-002, ECFA-04-230.
5. Beams for European Neutrino Experiments (BENE): Midterm scientific report. By BENE Steering Group (A. Baldini et al.). Jan 2006.
6. Bandyopadhyay A et al. (ISS Physics Working Group), Rept. Prog. Phys. 72 (2009) 106201
7. See also Guglielmi A, Mezzetto M, Migliozzi P and Terranova F, arXiv:hep-ph/0508034, published in Bettoni D et al., Phys. Rept. 434 (2006) 47. Battiston R, Mezzetto M, Migliozzi P and Terranova F, arXiv:0912.3372 [hep-ex].
8. Burguet-Castell J et al. Nucl. Phys. B 608 (2001) 301.

9. Apollonio M et al. (CHOOZ Collaboration), Eur. Phys. J. C 27 (2003) 331.
10. Schwetz T, Tortola M and Valle JWF, New J. Phys. 10, 113011 (2008)
11. Blondel A et al. Acta Phys. Polon. B 37 (2006) 2077.
12. Minakata H and Nunokawa H, JHEP 0110 (2001) 001.
13. Fogli GL and Lisi E, Phys. Rev. D 54 (1996) 3667.
14. Barger V, Marfatia D and Whisnant K, Phys. Rev. D 65 (2002) 073023.
15. Catanesi MG et al. (HARP Collaboration), Nucl. Instrum. Meth. A 571, 527 (2007).
16. Catanesi MG et al. (HARP Collaboration), Nucl. Phys. B 732, 1 (2006).
17. Catanesi MG et al. (HARP Collaboration), Eur. Phys. J. C 52, 29 (2007)
18. Huber P, Mezzetto M and Schwetz T, JHEP 0803, 021 (2008)
19. Ahn MH et al. (K2K Collaboration), Phys. Rev. Lett. 93 (2004) 051801.
20. The Fermilab NuMI Group, NumI Facility Technical Design Report Fermilab Report NuMI-346, 1998.
21. Adamson P et al. (MINOS Collaboration),
22. OPERA Collaboration, CERN-SPSC-P-318, LNGS-P25-00. Pessard H (OPERA Collaboration), arXiv:hep-ex/0504033. Guler M et al. (OPERA Collaboration), CERN-SPSC-2000-028.
23. Acquistapace G et al., CERN 98-02, INFN/AE-98/05 (1998); CERN-SL/99-034(DI), INFN/AE-99/05 Addendum.
24. Komatsu M, Migliozzi P and Terranova F, J. Phys. G 29 (2003) 443.
25. Itow Y et al., arXiv:hep-ex/0106019.
26. Ayres DS et al. (NOvA Collaboration), arXiv:hep-ex/0503053.
27. Ardellier F et al. (Double Chooz Collaboration), arXiv:hep-ex/0606025.
28. Guo X et al. (Daya Bay Collaboration), arXiv:hep-ex/0701029.

29. Mezzetto M, proceedings of "Venice 2009, Neutrino telescopes" 421-435, arXiv:0905.2842 [hep-ph].
30. Huber P et al. Nucl. Phys. Proc. Suppl. 145 (2005) 190. Huber P, Lindner M, Schwetz T and Winter W, JHEP 0911 (2009) 044
31. Mena O, Nunokawa H and Parke SJ, Phys. Rev. D 75 (2007) 033002.
32. Richter B, arXiv:hep-ph/0008222.
33. T. Kobayashi, J Phys G 29, 1493 (2003).
34. Kajita T, Minakata H, Nakayama S and Nunokawa H, Phys. Rev. D 75 (2007) 013006. Ishitsuka M, Kajita T, Minakata H and Nunokawa H, Phys. Rev. D 72 (2005) 033003.
35. Diwan M et al., arXiv:hep-ex/0608023.
36. Diwan MV et al., Phys. Rev. D 68 (2003) 012002
37. Autin B et al., CERN-2000-012. Garoby R, CERN-AB-2005-007.
38. http://paf.web.cern.ch/paf/. Bruning O et al., CERN-LHC-PROJECT-REPORT-626; W. Scandale, Nucl. Phys. Proc. Suppl. 154 (2006) 101.
39. Gomez-Cadenas JJ et al., Proceedings of Venice 2001, Neutrino telescopes vol. 2*, 463-481 [arXiv:hep-ph/0105297]. Blondel A et al., Nucl. Instrum. Meth. A 503 (2001) 173. M. Mezzetto, J. Phys. G 29 (2003) 1771. Apollonio M et al., arXiv:hep-ph/0210192. Campagne JE and Cazes A, Eur. Phys. J. C 45, 643 (2006)
40. Mezzetto M, Nucl. Phys. Proc. Suppl. 149 (2005) 179.
41. Mezzetto M, Nucl. Phys. Proc. Suppl. 143 (2005) 309.
42. Campagne JE, Maltoni M, Mezzetto M and Schwetz T, JHEP 0704 (2007) 003
43. de A Bellefon et al., arXiv:hep-ex/0607026.

44. D. Autiero et al., JCAP 0711 (2007) 011
45. Geer S, Phys. Rev. D 57 (1998) 6989 [Erratum-ibid. D 59 (1999) 039903]. Geer S, Ann. Rev. Nucl. Part. Sci. 59, 347 (2009).
46. Zucchelli P, Phys. Let. B, 532 (2002) 166-172.
47. Lindroos M and Mezzetto M, Imperial College Press, 2009, ISBN 978-1-84816-377-5.
48. Autin B et al, CERN/PS 2002-078 (OP), Nufact Note 121, Proceedings of Nufact 02, London, UK, 2002, J. Phys. G: Nucl. Part. Phys. 29 (2003) 1785-1795.
49. Albright C et al, Albright C et al, in APS Joint Study Report on the Future of Neutrino Physics, FNAL-TM-2259, 2004;
50. Ravn HR and Allardyce BW, On-Line Mass Separators, in Treatise on Heavy-Ion Science, Edt. Bromley DA, Plenum Press, New York, 1989, ISBN 0-306-42949-7.
51. Thiollière N et al, Internal note CEA, DAPNIA-06-274 and EURISOL note, 03-25-2006-0004.
52. Hass M et al, J. Physics G35, 104042 (2008).
53. Loislet M and Mitrofanov S, Oral presentation at the 6th Beta-beam Task Meeting, EURISOL, 19th November 2007, http://eurisol.org.
54. Rubbia C, Ferrari A, Kadi Y and Vlachoudis V, Nucl. Instrum. Meth. A 568 (2006) 475
55. Mori Y, Nucl. Instrum. and Methods A, 562 (2006) 591.
56. Reed C et al. in the proceedings the Seventh International Conference on Radioactive Nuclear Beams, Cortina d'Ampezzo, Italy, 2006.
57. Neuffer D, Fermi National Laboratory: Muon Collider and accelerator divi-

sion document database: NFMCC-doc-516, beams-doc-2856 (2007).

58. Sortais P et al. Rev Sci Instr 75 (2004) 1610.
59. http://www.ganil.fr/eurisol/
60. http://www.euronu.org
61. Lachaize A, Tkatchenko A, EURISOL DS task note 12-25-2008-0012.
62. Omet C et al. , New J. Phys. 8 (2006) 284.
63. Magistris M and Silari M, CERN technical note, CERN-TIS-2003-017-RP-TN.
64. A Chancé and Payet J, In the proceedings of EPAC, 2006, Edinburgh, UK, p.1933.
65. A Chancé and Payet J, In the proceedings of EPAC, 2008, Genoa, Italy. p.3104
66. Jones FW and Wildner E, in the proceedings of PAC07, Albuquerque, New Mexico, USA
67. Gupta R et al. IEEE Trans. Appl. Supercond. 14 (2004) 259.
68. Benedikt M and Hancock S, Nucl. Instrum. Meth. A 550 (2005) 1.
69. Hancock S, Lindroos M, McIntosh E and Metcalf M, Comput. Phys. Commun. 118 (1999) 61.
70. Hancock S, AIP Conf. Proc. 981 (2008) 89.
71. http://snowmass2001.org/
72. Källberg A and Lindroos M, EURISOL DS/TASK12/TN-05-04, http://eurisol.org and in the proceedings of European Particle Accelerator Conference, 2006, Edinburgh, Scotland.
73. Bernabeu J, Burguet-Castell J, Espinoza C and Lindroos M, JHEP 0512, 014 (2005)

74. Sato J, Phys. Rev. Lett. 95 (2005) 131804.

75. Fukumi A et al. arXiv:hep-ex/0612047.

76. Nacher E, Ph. D. Thesis, Univ. Valencia (2004).

77. Lindroos M, Bernabeu J, J Burguet-Castell and Espinoza C, In the proceedings of International Europhysics Conference on High energy Physics, Lisboa, Portugal, 2005, Proceedings of Science, http://pos.sissa.it/

78. Bosch F, GSI, Germany, 2005, private communication.

79. See for instance Masood SS et al. Phys. Rev. C 76 (2007) 045501

80. Mezzetto M, J. Phys. G 29 (2003) 1771

81. Bouchez J, Lindroos M and Mezzetto M, AIP Conf. Proc. 721 (2004) 37

82. Mezzetto M, Nucl. Phys. Proc. Suppl. 155 (2006) 214

83. Fernandez-Martinez E, arXiv:0912.3804 [hep-ph].

84. Ishihara C, arXiv:0912.1002 [hep-ex].

85. Burguet-Castell J et al. Nucl. Phys. B 695 (2004) 217

86. Huber P, Lindner M and Winter W, Comput. Phys. Commun. 167 (2005) 195. Huber P et al, Comput. Phys. Commun. 177, 432 (2007)

87. Huber P, Maltoni M and Schwetz T, Phys. Rev. D 71, 053006 (2005) Gandhi R et al. arXiv:hep-ph/0506145.

88. Burguet-Castell J et al. Nucl. Phys. B 725, 306 (2005)

89. Winter W, Phys. Rev. D 78 (2008) 037101

90. Huber P et al., Phys. Rev. D 73, 053002 (2006).

91. Terranova F, Marotta A, Migliozzi P and Spinetti M, Eur. Phys. J. C 38 (2004) 69.

92. Donini A et al. Eur. Phys. J. C 48, 787 (2006)

93. Rubbia C, arXiv:hep-ph/0609235.

94. Agarwalla SK and Huber P, arXiv:0909.2257 [hep-ph].

95. Donini A and Fernandez-Martinez E, Phys. Lett. B 641, 432 (2006)

96. Meloni D et al. JHEP 0807, 115 (2008)

97. Huber P and Winter W, Phys. Rev. D 68, 037301 (2003). Smirnov AY, arXiv:hep-ph/0610198. Minakata H, proceedings of "Venice 2007, Neutrino telescopes" 163-178 arXiv:0705.1009 [hep-ph].

98. Dziewonski AM and Anderson DL, Earth Phys Planet. Interiors 25, 297 (1981).

99. Agarwalla SK, Choubey S, Goswami S and Raychaudhuri A, Phys. Rev. D 75 (2007) 097302 Agarwalla SK, Choubey S and Raychaudhuri A, Nucl. Phys. B 771, 1 (2007) Agarwalla SK, Choubey S and Raychaudhuri A, Nucl. Phys. B 798, 124 (2008)

100. See http://www.imsc.res.in/∼ino.

101. Coloma P, Donini A, Fernandez-Martinez E and Lopez-Pavon J, JHEP 0805, 050 (2008)

102. Agarwalla SK, Choubey S, Raychaudhuri A and Winter W, JHEP 0806 (2008) 090

103. Choubey S, Coloma P, Donini A and Fernandez-Martinez E, JHEP 0912 (2009) 020

104. Agarwalla SK, Choubey S and Raychaudhuri A, Nucl. Phys. B 805 (2008) 305

105. Bernabeu J and Espinoza C, Phys. Lett. B 664, 285 (2008) Bernabeu J et al. JHEP 0906 (2009) 040

106. Rolinec M and Sato J, JHEP 0708, 079 (2007)

107. J. N. Bahcall, Phys. Rev. 194, 495 (1961).

108. Volpe C, J. Phys. G 30 (2004) L1 Volpe C, Nucl. Phys. Proc. Suppl. 155 (2006) 97
109. Serreau J and Volpe C, Phys. Rev. C 70 (2004) 055502. Volpe C, Nucl. Phys. Proc. Suppl. 143 (2005) 43
110. McLaughlin GC, Phys. Rev. C 70 (2004) 045804
111. Volpe C, J. Phys. G 31 (2005) 903
112. Lazauskas R and Volpe C, Nucl.Phys.A792:219-228,2007,
113. McLaughlin GC and Volpe C, Phys. Lett. B 591 (2004) 229
114. Balantekin AB, de Jesus JH and Volpe C, Phys. Lett. B 634 (2006) 180
115. Balantekin AB, de Jesus JH, R Lazauskas and Volpe C, Phys. Rev. D 73 (2006) 073011
116. Jachowicz N and McLaughlin GC, Phys. Rev. Lett. 96 (2006) 172301
117. Jachowicz N, McLaughlin GC and Volpe C, Phys. Rev. C 77 (2008) 055501
118. Lazauskas R, Balantekin AB, de Jesus JH and Volpe C, Phys. Rev. D 76 (2007) 053006
119. Amanik PS and McLaughlin GC, Phys. Rev. C 75, 065502 (2007)
120. Cocco AG et al. JCAP 0412 (2004) 002
121. Volpe C, Welzel J, arXiv:0711.3237.
122. Engel J, McLaughlin GC and Volpe C, Phys. Rev. D 67 (2003) 013005
123. Balantekin AB and Fuller GM, J. Phys. G 29, 2513 (2003)
124. Horowitz CJ, Phys. Rev. D 65, 043001 (2002)
125. Meyer BS, McLaughlin GC and Fuller GM, Phys. Rev. C 58, 3696 (1998)
126. Ruffert M, Janka HT, Takahashi K and Schaefer G, Astron. Astrophys. 319 (1997) 122
127. Kneller JP, McLaughlin GC and Surman R, J. Phys. G 32, 443 (2006)

128. Vogel P and Beacom JF, Phys. Rev. D 60, 053003 (1999)

129. Beacom JF, Farr WM and Vogel P, Phys. Rev. D 66 (2002) 033001

130. Bueno A, Carmona MC, Lozano J and Navas S, Phys. Rev. D 74, 033010 (2006).

131. Barranco J, Miranda OG and Rashba TI, Phys. Rev. D 76, 073008 (2007)

132. Agarwalla SK, Huber P and Link JM, arXiv:0907.3145 [hep-ph].

133. Volpe C, J. Phys. G 34 (2007) R1. See also Volpe C, Nucl. Phys. A 752 (2005) 38

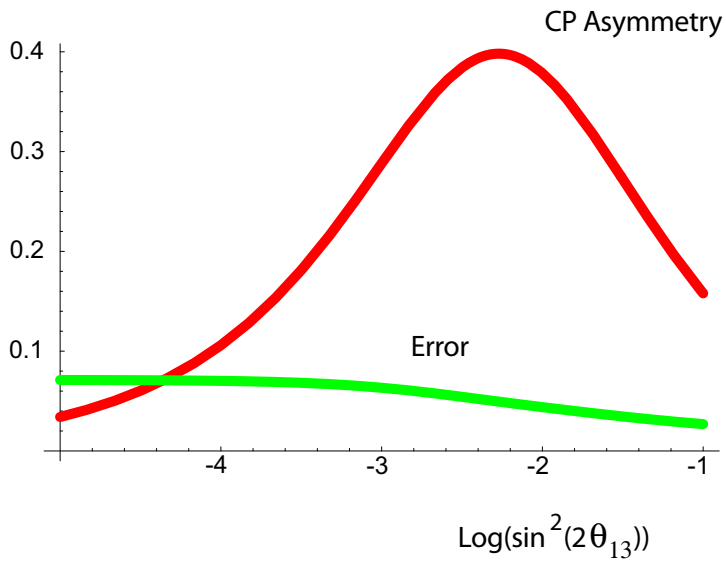

Figure 1: Magnitude of the CP asymmetry at the first oscillation maximum, for $\delta = 1$ as a function of the mixing angle $\sin^2 2\theta_{13}$. The curve marked "error" indicates the dependence of the statistical+systematic error on such a measurement. The curves have been computed for the baseline beta beam option at the fixed energy $E_\nu = 0.4$ GeV, $L = 130$ km, statistical + 2% systematic errors. From (11).

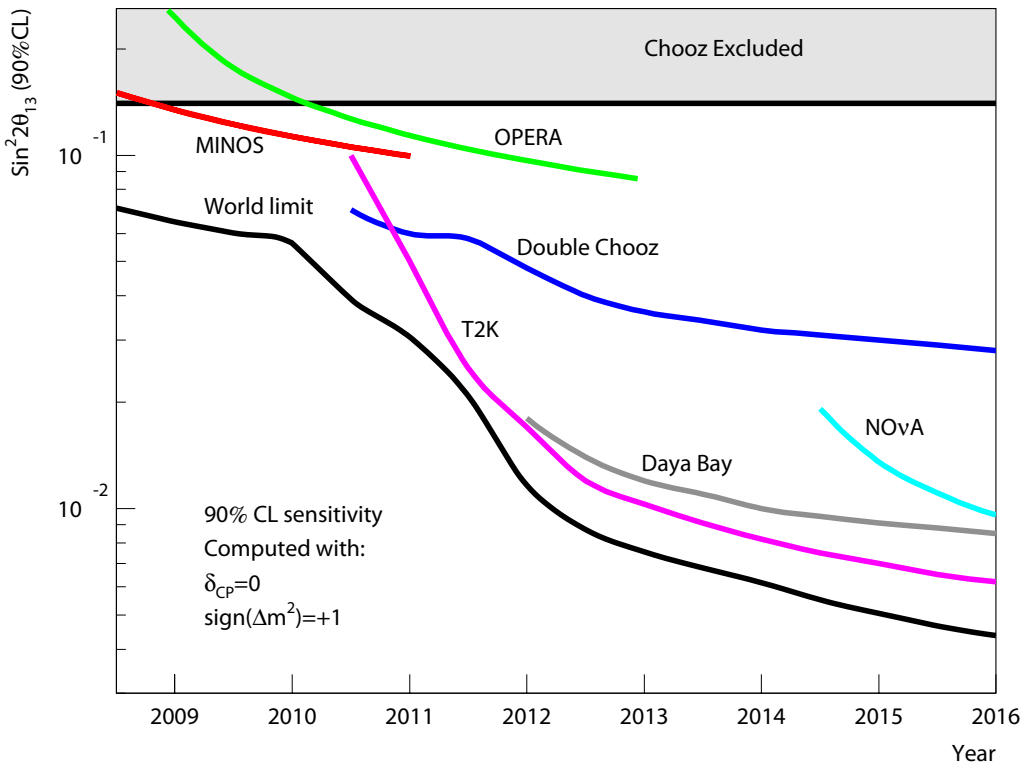

Figure 2: Evolution of experimental $\sin^2 2\theta_{13}$ sensitivities as function of time, computed assuming $\delta_{\rm CP} = 0$. Experiments are assumed to provide results after the first year of data taking, from (29)

.

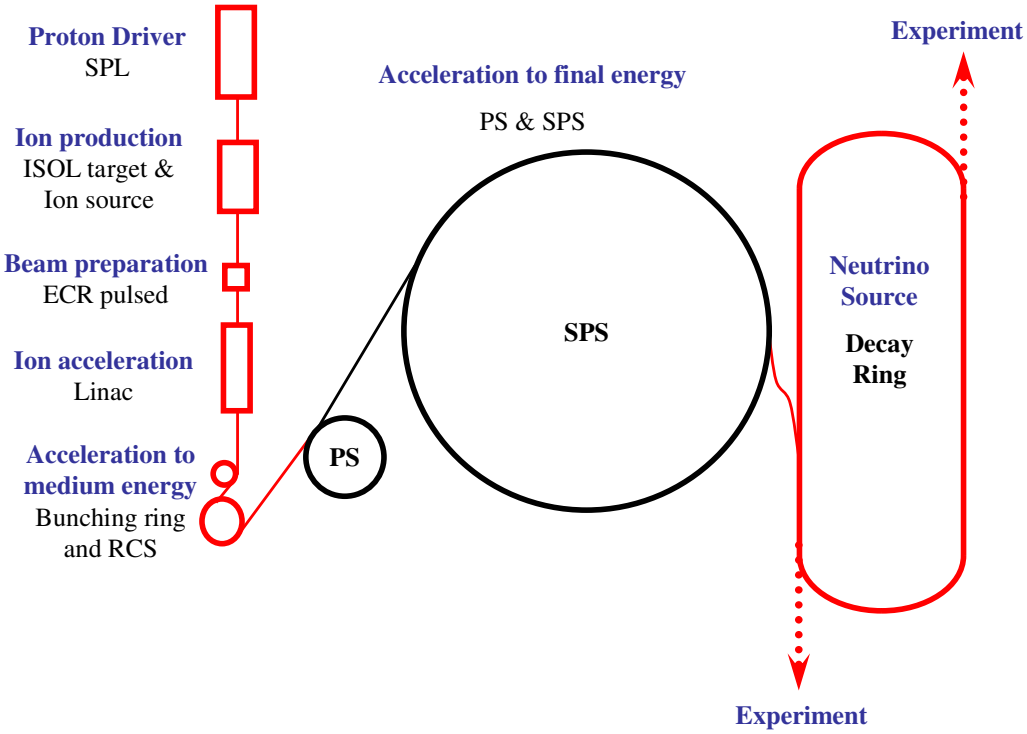

Figure 3: An overview of a possible beta-beam facility at CERN as discussed in (48). Note that the existing accelerators PS and SPS were proposed as part of the injector chain, this represents a major saving for the proposal.

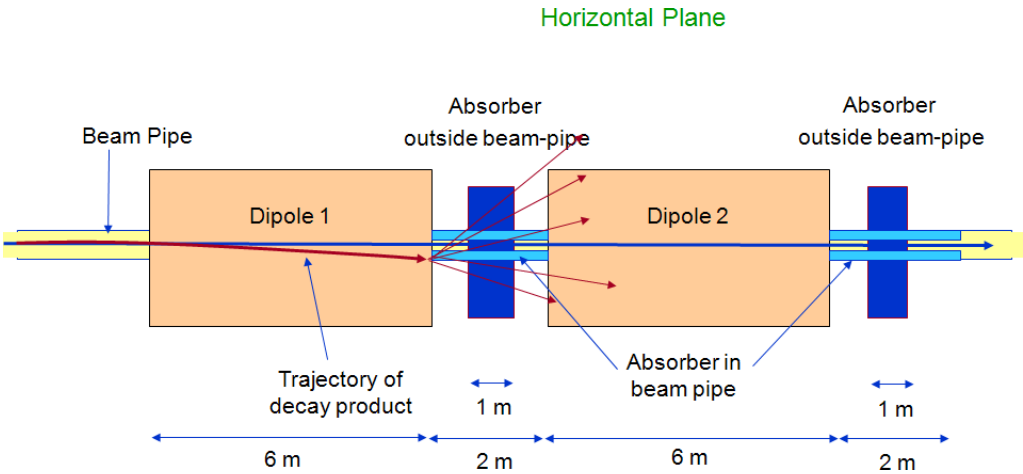

Figure 4: The beam loss from radioactive decay in the arcs cannot be avoided and the dipoles must be adapted in length so that the daughter products are lost in absorbers between the dipoles and not in the dipoles themselves.

Table 1: Some possible isotopes which are β^- emitters, from (48)

Isotope	A/Z	$T_{1/2}$ (s)	Q_β g.s. to g.s. (MeV)	Q_β effective (MeV)	E_β average (MeV)	$E\nu$ average (MeV)
^{6}He	3.0	0.80	3.5	3.5	1.57	1.94
^{8}He	4.0	0.11	10.7	9.1	4.35	4.80
^{8}Li	2.7	0.83	16.0	13.0	6.24	6.72
^{9}Li	3.0	0.17	13.6	11.9	5.73	6.20
^{11}Be	2.8	13.8	11.5	9.8	4.65	5.11
^{15}C	2.5	2.44	9.8	6.4	2.87	3.55
^{16}C	2.7	0.74	8.0	4.5	2.05	2.46
^{16}N	2.3	7.13	10.4	5.9	4.59	1.33
^{17}N	2.4	4.17	8.7	3.8	1.71	2.10
^{18}N	2.6	0.64	13.9	8.0	5.33	2.67
^{23}Ne	2.3	37.2	4.4	4.2	1.90	2.31
^{25}Ne	2.5	0.60	7.3	6.9	3.18	3.73
^{25}Na	2.3	59.1	3.8	3.4	1.51	1.90
^{26}Na	2.4	1.07	9.3	7.2	3.34	3.81

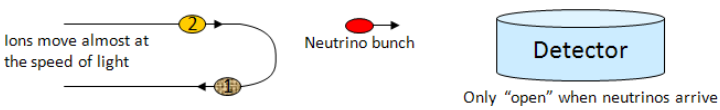

Figure 5: The neutrino beam from the beta-beam facility will have a bunched structure which mirrors the bunch structure of the ion-beam. In the figure, the neutrino bunch originates from the ion bunch marked with a 1, the neutrinos from the decay of ions in the bunch marked 2 has not left the ring yet but are traveling along the straight section with the same velocity as the ions.

Table 2: Some possible isotopes which are β^+ emitters, from (48)

Isotope	A/Z	$T_{1/2}$ (s)	Q_β g.s. to g.s. (MeV)	Q_β effective (MeV)	E_β average (MeV)	$E\nu$ average (MeV)
^{8}B	1.6	0.77	17.0	13.9	6.55	7.37
^{10}C	1.7	19.3	2.6	1.9	0.81	1.08
^{14}O	1.8	70.6	4.1	1.8	0.78	1.05
^{15}O	1.9	122.	1.7	1.7	0.74	1.00
^{18}Ne	1.8	1.67	3.3	3.0	1.50	1.52
^{19}Ne	1.9	17.3	2.2	2.2	0.96	1.25
^{21}Na	1.9	22.4	2.5	2.5	1.10	1.41
^{33}Ar	1.8	0.17	10.6	8.2	3.97	4.19
^{24}Ar	1.9	0.84	5.0	5.0	2.29	2.67
^{35}Ar	1.9	1.77	4.9	4.9	2.27	2.65
^{37}K	1.9	1.22	5.1	5.1	2.35	2.72
^{80}Rb	2.2	34	4.7	4.5	2.04	2.48

Table 3: Estimates made by the authors for the production rate in the target for a few beta-beam isotopes. The extraction efficiency from the target can vary considerably from a few percent up to 90%. The references refers to the method rather than to the production limits.

Isotope	Method	Rate within reach ions/second	Refe
^{18}Ne	ISOL at 1 GeV and 200 kW	$< 8 \times 10^{11}$	(48)
^{6}He	ISOL converter at 1 GeV and 200 kW	$< 5 \times 10^{13}$	(48)
^{18}Ne	Direct production through ^{16}O(^{3}He,n)^{18}Ne	$< 1 \times 10^{13}$	(53)
^{6}He	ISOL converter at 40 MeV Deuterons and 80 kW	$< 6 \times 10^{13}$	(52)
^{8}Li	Production ring through ^{7}Li(d,p)^{8}Li	$< 1 \times 10^{14}$	(54)

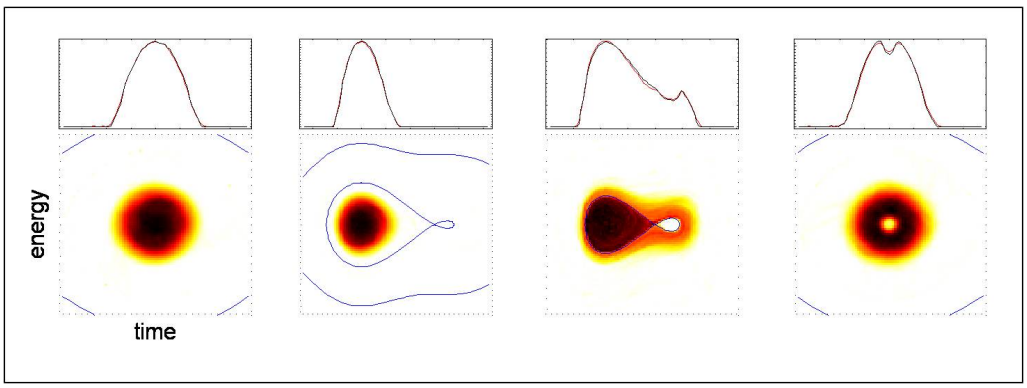

Figure 6: The stacking scheme was tested in the CERN PS ((68)) where an high intensity proton beam was merged with s small part of empty phase space with high efficiency. In the top part of the figure the line current for the bunches during the merging process and in the bottom part the tomographic (69) reconstruction of the bunches are shown.

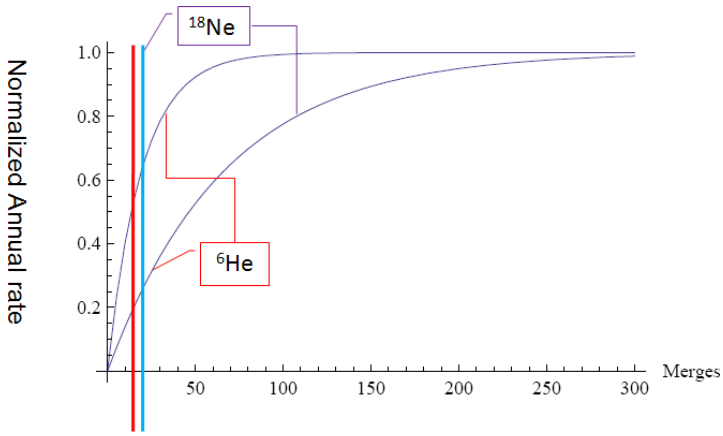

Figure 7: In the diagram the fraction of ^{6}He ions (upper line) and ^{18}Ne ions (lower line) stored in the decay ring using the stacking scheme discussed in subsection 2.6 are plotted as a function of the number of 100% efficient merges. The ideal case to which the curves eventually converge is the ideal case in which all ions are accumulated in the ring until they decay. The vertical lines for each ion types marks the stacking limits for the beta-beam studied in (48).

Table 4: Some decay ring options for a different Lorenz gamma of ^{6}He. The decay ring arcs are for all cases considered to be completely filled with dipoles.

Gamma	Rigidity [Tm]	Ring length[a]	Dipole Field[b]
100	935	4197	3.1
150	1403	6296	4.7
200	1870	8395	6.2
350	3273	14691	10.9
500	4676	20987	15.6

[a]Assuming a fixed field of 5 T and a single straight section of 36% of the circumference

[b]Assuming a arc radius of 300 m and a decay ring length of 6885 m

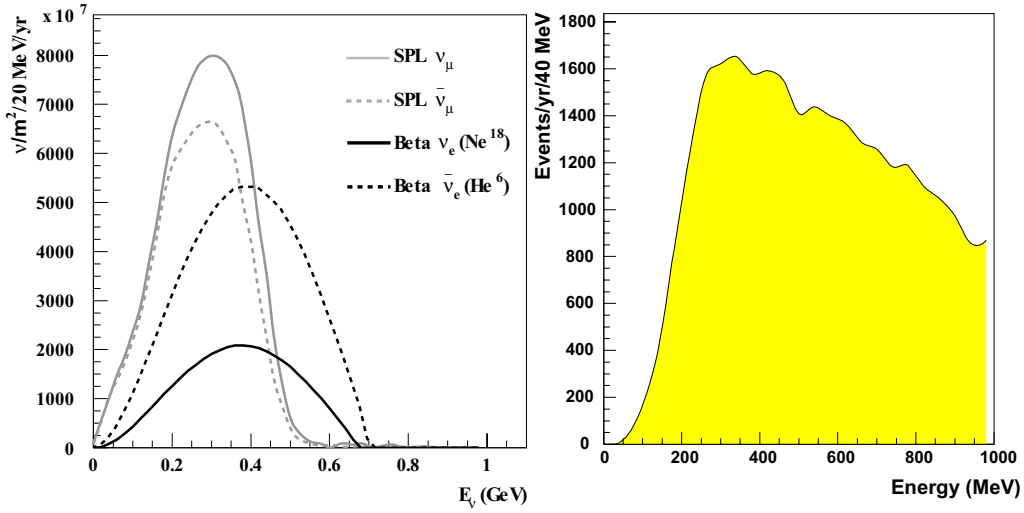

Figure 8: Left panel: neutrino flux of β-Beam ($\gamma = 100$) together with the CERN-SPL super beam, at 130 km of distance. Right panel: rate of atmospheric $\nu_\mu + \overline{\nu}_\mu$ interactions in MEMPHYS, integrated in one year.

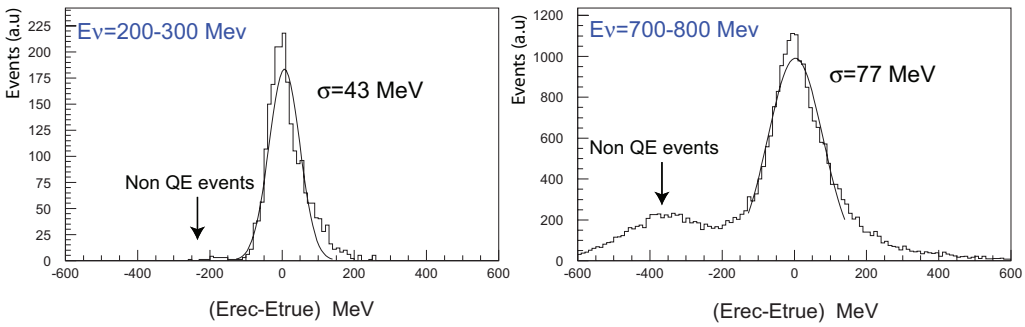

Figure 9: Energy resolution for ν_e interactions in the 200–300 MeV and 700–800 MeV energy ranges. The quantity displayed is the difference between the reconstructed and the true neutrino energy.

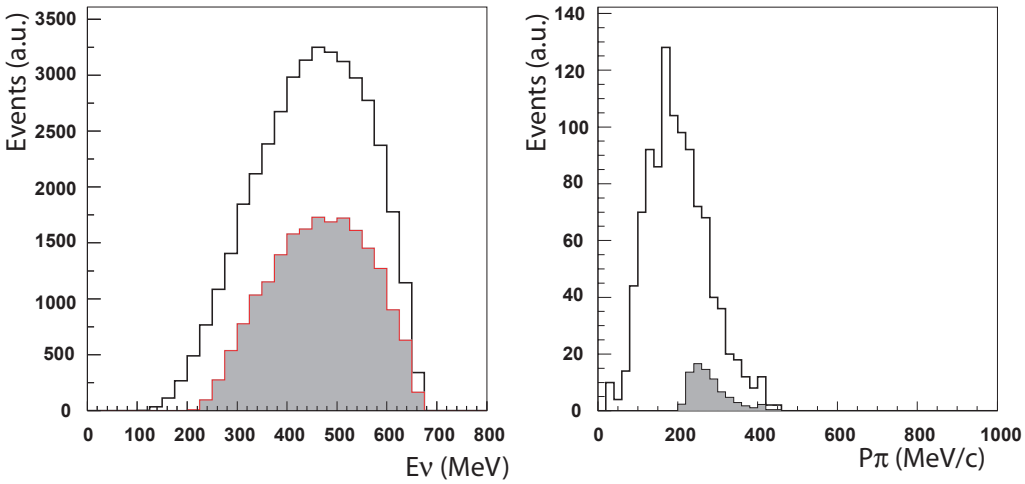

Figure 10: Left: Event reduction for ^{18}Ne oscillated events (left) and pion background, $\pi^+ + \pi^-$ (right).

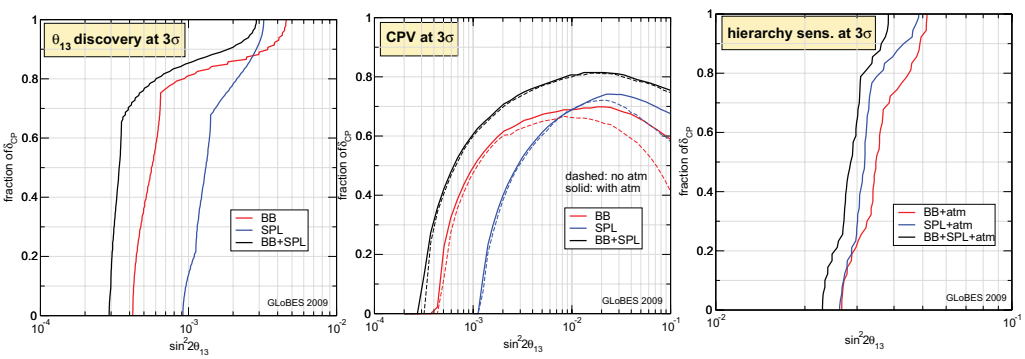

Figure 11: 3σ sensitivities for CFBB (red curve), the SPL super beam (blue curve) and their combination (black curve), including or not the atmospheric neutrino data (solid and dashed lines respectively). Computed as a function of the fraction of all possible values of $\delta_{\rm CP}$. Left panel: sensitivity to θ_{13}, central panel: sensitivity to leptonic CP violation, right panel: sensitivity to the mass hierarchy, adapted from (42) (courtesy of T. Schwetz).